Nucleic Acids Research, 2026, **54**, gkaf1512
https://doi.org/10.1093/nar/gkaf1512
Nucleic Acid Enzymes

Tho1 and MOS11 promote nucleic acid double-strand unwinding by facilitating DEAD-box helicase oligomerization

Fabienne Becker[1], Matthias Bastian Miosga[1], Minhaz Mannan[1,2], Vera Bettenworth[1], Wieland Steinchen[3], Katja Sträßer[1,4], Peter Friedhoff[1,*]

[1]Justus Liebig University Giessen, Institute of Biochemistry, Heinrich-Buff-Ring 17, 35392 Giessen, Germany
[2]Heidelberg University Hospital, Department of Internal Medicine, Im Neuenheimer Feld 410, 69120 Heidelberg, Germany
[3]Philipps University Marburg, Center for Synthetic Microbiology (SYNMIKRO), Karl-von-Frisch-Straße 14, 35043 Marburg, Germany
[4]Cardio-Pulmonary Institute (CPI), EXC 2026, 35392 Giessen, Germany

*To whom correspondence should be addressed. Email: peter.friedhoff@chemie.bio.uni-giessen.de

Abstract

DEAD-box helicases are essential for gene expression and RNA metabolism. However, the mechanisms regulating their activity remain largely elusive. The DEAD-box helicase DDX39B/UAP56 forms a 2:1 complex with the C-terminal domain (CTD) of RNA-binding protein Tho1, but the functional relevance of this interaction is still elusive. Here, we show that the Tho1-CTD stimulates the helicase activity of Sub2, the yeast homologue of DDX39B/UAP56, by acting as a rigid scaffold that promotes Sub2 oligomerization on RNA. The Tho1-CTD has two conserved α-helical motifs, each interacting with one Sub2, and we demonstrate that both motifs are essential for the stimulation. This scaffolding mechanism is shared across species, as the Tho1 ortholog MOS11 from *Arabidopsis thaliana* stimulates *A. thaliana* UAP56. Interestingly, MOS11 has five of the conserved α-helical motifs, which are connected by flexible linkers. We show that the number and spatial separation of these motifs are critical for stimulation and that MOS11 stimulates unwinding on a broader range of substrates than the Tho1-CTD. The cofactor-mediated helicase oligomerization is reminiscent of the self-oligomerization observed for other DEAD-box helicases. Furthermore, our data illustrate how cofactor architecture affects substrate specificity and provide a comprehensive mechanistic framework for cofactor-mediated helicase activation.

Graphical abstract

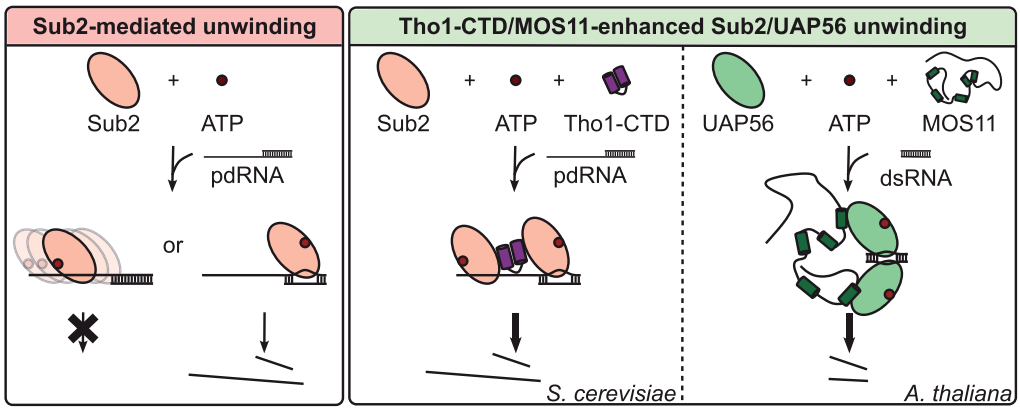

Introduction

DEAD-box helicases form the largest group of RNA helicases and play central roles in all steps of RNA metabolism [1, 2]. Unlike processive helicases that translocate along their nucleic acid substrates to separate double-stranded regions, DEAD-box helicases unwind RNA duplexes by a local strand separation mechanism that does not involve translocation [3]. Instead, they bind RNA in an ATP-dependent manner, leading to the destabilization of double-stranded structures and subsequent strand separation [1, 4]. The unwinding efficiency of DEAD-box helicases is affected by several factors, including the length and stability of the double-strand, the presence of single-stranded extensions to the duplex [5–9] and, in some cases, helicase oligomerization [10–12]. Furthermore, DEAD-

Received: March 18, 2025. **Revised:** December 8, 2025. **Accepted:** December 18, 2025

box helicases are often part of large multisubunit complexes [1] in which their ATPase activity and/or RNA affinity are regulated by other proteins [13–15]. However, the underlying mechanisms as well as the specific contributions to cellular processes of many DEAD-box helicases are often not fully understood.

The DEAD-box helicase Sub2 from *Saccharomyces cerevisiae* (ortholog of human DDX39B/UAP56) is involved in multiple steps of gene expression, including mRNA splicing, 3′ end processing, and nuclear mRNA export as a component of the conserved TREX complex [16–20]. In addition to Sub2, TREX consists of the heteropentameric THO complex (Tho2, Hpr1, Mft1, Thp2, and Tex1), the RNA annealing protein Yra1 (ALYREF in humans) and the SR-like proteins Gbp2 and Hrb1 [20, 21]. Defects in the THO complex, Yra1 or Sub2 cause a nuclear mRNA export defect, increased recombination and genome instability—the latter of which is often linked to RNA:DNA hybrid (R-loop) formation [8, 22, 23]. Within the TREX complex, Sub2's activity is regulated by its interactions with Yra1 and the THO complex [24–26].

Another interaction partner of Sub2 is Tho1, a protein also involved in mRNP biogenesis [27]. Deletion of *MOS11*, the Tho1 ortholog in *Arabidopsis thaliana*, leads to a nuclear mRNA export defect [28]. The human Tho1 ortholog SARNP (also CIP29) is essential for nuclear mRNA export and cell viability and is upregulated in cancer cells [29, 30]. In contrast, deletion of *THO1* in *S. cerevisiae* has no apparent phenotype [27]. However, overexpression of either Tho1 or Sub2 suppresses the hyperrecombination phenotype as well as the nuclear mRNA export and growth defects in cells with a defective THO complex [27, 31, 32]. This suggests that the cellular functions of Tho1 and Sub2 either overlap or that Tho1 exerts this effect by enhancing Sub2's activity. Indeed, both SARNP and MOS11 stimulate the helicase activity of their respective Sub2 orthologs through a hitherto unknown mechanism [25, 26, 33, 34].

A direct interaction between the C-terminal domain (CTD) of Tho1 and Sub2 was predicted in a proteome-wide 3D structure modelling effort covering >900 potential yeast protein complexes [35]. This prediction was later supported by a co-crystal structure, which revealed a 2:1 complex formed by human DDX39B/UAP56 with the Tho1-CTD from *S. cerevisiae* [36]. The interaction is mediated by a tandem repeat of an α-helical motif of Tho1 that is conserved in the Tho1 orthologs SARNP and MOS11 [36, 37] and has been termed DDX39B interacting motif [36] or UAP56 clamping motif [38]. While the two motifs within the Tho1-CTD are connected by a short linker and constitute two antiparallel helices, the orthologs contain a larger number of helical motifs connected by flexible linkers, allowing for more structural diversity [36, 37]. However, the functional significance of this interaction and the role of multiple helical motifs in Tho1 orthologs remain elusive.

Here, we demonstrate that the Tho1-CTD is sufficient to suppress the thermosensitive (ts) phenotype of cells lacking the THO complex component Hpr1. Importantly, the Tho1-CTD enhances Sub2's helicase activity by serving as a scaffold that bridges two helicase protomers on an RNA substrate. Single point mutations in either one of the conserved interaction motifs, restricting complex formation to a 1:1 stoichiometry, abolishes this stimulation as well as the ts phenotype suppression. Likewise, the *A. thaliana* ortholog MOS11 requires at least two of its helical motifs to stimulate UAP56's helicase activity. However, compared to the Tho1-CTD, MOS11 exerts this stimulation across a broader range of RNA substrates, probably either due to the larger motif number or due to their greater three-dimensional flexibility. Together, our findings suggest an evolutionarily conserved mechanism for helicase activation: a cofactor-mediated oligomerization in which the cofactor's architecture specifies the substrate range.

Materials and methods

Cloning

Escherichia coli strains, plasmids, and primers are listed in Supplementary Tables S2–S4, respectively. Genes encoding Sub2 and Tho1 wild-type proteins were amplified from *S. cerevisiae* (W303) genomic DNA. cDNA from *A. thaliana* for amplification of the gene encoding UAP56 and MOS11 was generously provided by Prof. Dr Karl-Heinz Kogel (Justus Liebig University Giessen). Mutants were constructed based on the published Sub2/DDX39B:Tho1-CTD interface [35, 36]. Cloning was done by Gibson Assembly. The *pT7* expression vector for protein expression in *E. coli* introduces a hexa-histidine (6xHis) tag followed by a TEV cleavage site (ENLYFQG) at the N-terminus of the respective protein. For overexpression of Tho1 variants in yeast cells, the high-copy plasmid pRS424 was used. For genomic integration of *THO1* variants, PCR fragments containing flanking regions homologous to the endogenous *THO1* locus were amplified from plasmid YEpGal (Supplementary Fig. S14A) and used for homologous recombination. All DNA sequences were verified by Sanger sequencing.

Yeast strains

Yeast strains are listed in Supplementary Table S5. All strains derived from strain W303 are referred to as wild type.

Dot spot assay

For dot spot assays shown in Fig. 1, 10-fold serial dilutions of wild-type and *Δhpr1* cells transformed with the high-copy vector pRS424 expressing Tho1 or the Tho1-CTD were spotted onto SDC (-trp) plates and grown at the indicated temperatures. For dot spot assays in Fig. 4, THO1-CTD variants were overexpressed from the GAL promoter via integration at the endogenous *THO1* locus (Supplementary Fig. S14). The plates were imaged after 3 days. Quantification of dot spots was performed as described in [39, 40].

Western blot

To verify the expression of Tho1 mutants, wild-type and *Δhpr1* cells were grown in SDC (-trp) medium to an OD_{600} of 0.6 and harvested. Cell pellets were lysed using alkaline lysis and proteins precipitated with TCA [41]. Total protein was separated by sodium dodecyl sulfate-polyacrylamide gel electrophoresis (SDS–PAGE) and transferred onto a nitrocellulose membrane (Porablot, Macherey, and Nagel). The respective primary antibody and a horse-radish peroxidase-coupled secondary antibody were applied. For visualization, CheLuminate-HRP PicoDetect ECL kit (AppliChem) and ChemoCam Imager (Intas) were used. The following primary antibodies were used: Pgk1 monoclonal antibody (22C5D8, 459 250, Invitrogen) and Tho1 polyclonal antibody (Pineda Lab).

Protein purification

His-tagged proteins were expressed in *E. coli* Rosetta (DE3) cells and grown in LB medium containing respective antibiotic for selection (25 μg/ml). Bacteria were grown at 37°C to an OD_{600} of 0.7, induced with 1 mM isopropyl beta-D-thiogalactoside (IPTG) and cultured overnight at 20°C. Harvested cells were lysed in lysis buffer [50 mM HEPES pH 7.5, 150 mM KCl, 10% (v/v) glycerol, 0.15% (v/v) NP-40, and 15 mM imidazole] by sonication, followed by ultracentrifugation (164 700 RCF at 4°C for 45 min). The supernatant was subjected to nickel affinity purification with Protino® Ni-IDA columns (Macherey–Nagel). Columns were washed five times with buffers of varying KCl concentrations (300, 500, 700, 1000, and again 150 mM), and proteins were eluted with elution buffer containing imidazole [50 mM HEPES pH 7.5, 150 mM KCl, 10% (v/v) glycerol, and 250 mM imidazole]. For Sub2 and UAP56, protein-containing fractions were incubated with TEV protease overnight at 4°C. To remove the TEV protease and nonspecific proteins, gel filtration was performed with a Superdex 200 10/300 GL (Cytiva) column in gel filtration buffer [50 mM HEPES, pH 7.5, 50 mM KCl, 10% (v/v) glycerol]. All buffers for Sub2/UAP56 purification contained 2 mM of TCEP. For Tho1-CTD and MOS11 variants, Ni-IDA fractions were buffer-exchanged into gel filtration buffer using Zeba Spin desalting columns (10K MWCO, Thermo Fisher Scientific). The His-tag was cleaved by TEV protease overnight at 4°C. To remove the His-tagged TEV protease and remaining His-tagged proteins, samples were passed through Ni-NTA Agarose (Macherey-Nagel) and further purified by gel filtration with a Superdex 75 10/300 GL (Cytiva) column. All purified proteins were flash-frozen in liquid nitrogen and stored at −80°C. Protein concentration was measured using NanoDrop for Sub2 and UAP56 or BCA assay for Tho1-CTD and MOS11 variants.

RNA substrate preparation

Oligonucleotides used for the helicase assays were designed based on the sequences published in [42, 43] and are listed in Supplementary Table S6. For (partial) duplex nucleic acid substrates, complementary RNA or DNA strands were combined in a 1:1 ratio at 1 μM each in annealing buffer (10 mM HEPES, pH 7.5, 50 mM KCl). The mixture was heated to 95°C for 10 min in a thermocycler, then gradually cooled by 5°C increments every 5 min until reaching 4°C.

Real-time fluorescence unwinding assay

The real-time fluorescence helicase assay was modified according to [44]. The 13 nt top strands were labelled with 6-FAM or BHQ-2, 13 nt and 38 nt bottom strands with Cy5. Reactions were carried out at 23°C in a 96-well plate (Greiner 96 Flat Bottom Black Polystyrene) using Tecan Infinite F Plex plate reader. Fluorescence from the 6-FAM donor ($F_{D|D}$) was measured at 535 nm (25 nm bandwidth) with excitation at 485 nm (20 nm bandwidth). Cy5 (acceptor) fluorescence was measured at 670 nm (20 nm bandwidth), either with excitation at 620 nm (10 nm bandwidth) as $F_{A|A}$, or with excitation at 535 nm as $F_{A|D}$ [45]. Strand separation was monitored by increasing $F_{D|D}$ intensity and decreasing $F_{A|D}$ intensity. Fraction duplex was calculated by normalizing the buffer-corrected acceptor fluorescence signal after donor excitation ($F_{A|D}$) to signals of reactions without protein. Donor bleed-through and acceptor crosstalk was measured and found to be negligible (see Supplementary Table S1 and Supplementary Fig. S3 for further information). Fluorescence anisotropy was measured at 535 nm (25 nm bandwidth) following excitation at 485 nm (20 nm bandwidth) [46]. For substrates containing BHQ-2 and Cy5, unwinding was measured by increasing Cy5 intensities using an excitation wavelength of 620 nm (10 nm bandwidth) and emission wavelength of 670 nm. Fraction unwound was calculated by normalizing measured Cy5 intensities to signal obtained from a Cy5-labelled 38 nt RNA. Unless stated otherwise, Sub2/UAP56 in a final concentration of 1 μM in 200 μl was pre-incubated for 10 min in 90 μl helicase buffer (50 mM HEPES–KOH, pH 7.5; 4 mM TCEP, pH 7.0) containing 2 mM ATP and 1 mM $MgCl_2$. Reactions were carried out under multiround conditions and started by addition of 100 μl substrate solution (final concentration 10 nM). For two-phase measurements, unwinding stimulation was initiated after 15 min by addition of 10 μl Tho1-CTD/MOS11 solution (final concentration 2 μM) and reactions were monitored for another 45 min.

Stopped-flow measurements for fast unwinding kinetics

To capture the initial seconds of fast unwinding reactions, experiments were conducted using a stopped-flow device (SF-61SX2, TgK Scientific, Bradford-on-Avon, UK) with an LED light source (LED L470A with prefilter SP OD4 500 nm, 12.5 mm) for excitation. Donor fluorescence was detected using an ET525/50 band-pass filter (Chroma Technology, Olching, Germany), and acceptor fluorescence with an ET670/50 band-pass filter (Chroma Technology). Buffer conditions were the same as in the plate reader assay. Syringe 1 contained 2 μM Sub2 with or without 1 μM Tho1-CTD, preincubated for 10 min. Syringe 2 contained 20 nM RNA substrate. Reactions were initiated by mixing the contents of both syringes in a 1:1 ratio, resulting in final concentrations of 1 μM Sub2, 0.5 μM Tho1-CTD, and 10 nM RNA. Unwinding was monitored over a 5-min period. Data were analysed using Origin Pro (version 2024b; OriginLab Corporation, Northampton, MA, USA). Fraction duplex was calculated by normalizing buffer-corrected fluorescence values to the initial signal at the start of the reaction.

Heterobifunctional crosslinking

Heterobifunctional crosslinking with S-{4-[(2,5-Dioxo-1-pyrrolidinyl)oxy]-4-oxobutyl} methanesulfonothioate (MTS-4-NHS, Biozol) was performed following a protocol adapted from [47]. The reaction was conducted in 20 μl of crosslinking buffer [50 mM HEPES, pH 7.5, 50 mM KCl, 10% (v/v) glycerol, 0.5 mM $MgCl_2$] with or without 1 mM AMPPNP and 2.5 μM 38 nt RNA. UAP56 (5 μM) and Tho1-CTD (2.5 μM) were incubated together for 3 min. Unless otherwise specified, the crosslinking reaction was initiated by adding 500 μM MTS-4-NHS and terminated after 5 min by adding Tris-containing 4× SDS loading dye [250 mM Tris–HCl, pH 6.8, 9% (w/v) SDS, 40% (v/v) glycerol, 0.2% (w/v) bromophenol blue]. The samples were boiled for 2 min at 95°C and 17 μl of the reaction loaded onto a 12% SDS–PAGE gel. Protein bands were visualized using Coomassie blue staining.

Electrophoretic mobility shift assay

Electrophoretic mobility shift assay (EMSA) experiments were performed to test ternary complex formation. Sub2 mutants

(5 μM) and the Tho1-CTD (10 μM) were pre-incubated in 12 μl binding buffer [20 mM MES, pH 6.5, 4 mM TCEP, 10% (v/v) glycerol] with 1 mM AMPPNP and 0.5 mM $MgCl_2$ for 10 min. 6-FAM-labelled 13 nt RNA (100 nM) was added to the reaction and incubated for 15 min. Samples were visualized after native polyacrylamide gel electrophoresis (10% polyacrylamide in TBE buffer) at 100 V for 75 min using imager Typhoon FLA 9500.

Statistical analysis

Data shown as mean ± standard deviation (error bars) derives from at least three independent replicates. Statistical significance was calculated using a two-sided Student's *t*-test with ∗: *P* value ≤ .05, ∗∗: *P*-value ≤ .01, and ∗∗∗: *P*-value ≤ .001. For statistical analysis of data in Fig. 7C and D and Supplementary Fig. 23, data were normalized to the control (UAP56, "–") within each experiment to account for batch effects. Fold change (FC) values represent the ratio of velocity in the presence of MOS11 variant to that of the control. Statistical significance was assessed using a one-sample *t*-test against a null mean of 1.0. *P*-values were corrected for multiple comparisons using the Benjamini–Hochberg procedure to control the false discovery rate (FDR). Significance levels are indicated as ∗: $P < .05$, ∗∗: $P < .01$, and ∗∗∗: $P < .001$. Data can be found in Supplementary Dataset 4.

Results

Overexpression of the Tho1-CTD suppresses the ts phenotype of *Δhpr1* cells

The conserved mRNP component Tho1 is an interaction partner of Sub2, and overexpression of either Tho1 or Sub2 suppresses phenotypes occurring in cells lacking the THO component Hpr1 [27, 31, 32] . Tho1 contains an N-terminal SAF-A/B, Acinus, and PIAS (SAP) domain (aa 4–38) (Fig. 1A), which binds DNA, but not RNA [27, 37]. A 168 aa Tho1 fragment (aa 51–218) lacking this domain binds RNA and, when overexpressed, suppresses the ts phenotype of *Δhpr1* cells [27]. In addition to two longer unstructured regions, this fragment includes Tho1's second structured domain, the CTD, which is composed of the two above-mentioned antiparallel α-helices with their highly conserved sequence motifs as well as a third, short, and not conserved helix [36, 37]. Since the interaction of this CTD with Sub2 might be crucial for the suppression of the growth defect occurring in *Δhpr1* cells, we assessed whether the Tho1-CTD (aa 117–183) suppresses the ts phenotype at 37°C. Indeed, overexpression of the Tho1-CTD supresses the growth defect of *Δhpr1* cells similarly to the overexpression of full-length Tho1 (Fig. 1B and C and Supplementary Fig. S1). Thus, the Tho1-CTD is sufficient for suppression of the ts phenotype of *Δhpr1* cells.

The Tho1-CTD stimulates unwinding of RNA duplexes by Sub2

To assess how the Tho1-CTD suppresses the ts phenotype of *Δhpr1* cells, we tested its effect on Sub2's helicase activity, since the Tho1 orthologs SARNP (human) and MOS11 (*A. thaliana*) stimulate the helicase activity of their respective Sub2 orthologs, DDX39B/UAP56 in human and UAP56 in *A. thaliana* [25, 26, 34]. To determine helicase activity, we used a real-time unwinding assay based on the decrease in the FRET from the donor dye 6-carboxyfluorescein (6-FAM), attached to the shorter strand, to the acceptor dye cyanine 5 (Cy5), attached to the longer strand, of a partial duplex RNA (pdRNA) (Fig. 2A and Supplementary Figs S2 and S3) [48, 49]. Unwinding of this substrate was monitored for 15 min in the presence of Sub2 (phase 1). Then, either buffer or the Tho1-CTD was added, and unwinding measured for further 45 min (phase 2). In addition, fluorescence anisotropy of 6-FAM was measured over the whole assay to monitor protein-RNA binding (Supplementary Fig. S4A and B).

The Tho1-CTD alone neither bound to the pdRNA nor led to its unwinding (Fig. 2B and Supplementary Fig. S4A), consistent with the report that a recombinant protein mainly consisting of this CTD (aa 119–183) exhibits no potential to bind RNA [37]. Sub2 alone bound the pdRNA almost immediately (<1 min), but unwinding was slow. Importantly, addition of the Tho1-CTD increased the extent of unwinding by Sub2 by twofold without affecting RNA binding (Fig. 2B and D and Supplementary Figs S2B and S4A). The observed stimulation was concentration-dependent, reaching maximum at micromolar Tho1-CTD concentrations (Supplementary Fig. S5). Notably, the fluorescence anisotropy did not further increase upon addition of the Tho1-CTD and did not exceed the maximal values obtained for a single-stranded substrate (Supplementary Fig. S4B and C). Fluorescence anisotropy is influenced not just by the molecular mass of the nucleic acid-protein complex, but also by the local mobility of the fluorophore (such as 6-FAM) attached to the nucleic acid. The flexibility of the fluorophore's linker and its environment can allow significant local motion, reducing the observed anisotropy and masking the effects of global size changes [50]. Hence, the absence of a measurable additional change in anisotropy does not exclude association of the Tho1-CTD to the Sub2-pdRNA complex.

To rule out a fluorophore-specific effect caused by 6-FAM, stimulation of the Tho1-CTD on Sub2 was confirmed in a different setup using a pdRNA substrate with a 13 nt top strand labelled with a black hole quencher-2 (BHQ2) [44] (Supplementary Fig. S6). Taken together, we conclude that the Tho1-CTD stimulates Sub2's helicase activity.

The stimulation of Sub2's helicase activity by the Tho1-CTD depends on their direct interaction

Next, we investigated whether and if so, how, the observed stimulation depends on the physical interaction between Sub2 and the Tho1-CTD. To generate a Sub2 mutant deficient in Tho1-CTD binding, a structural model of the Tho1-Sub2 complex, which agrees well with the experimentally determined structure of the Tho1-CTD and human DDX39B/UAP56 (rmsd of 0.607 Å for Tho1-CTD and DDX39B aa 258–426), was used (Fig. 2C) [35, 36]. Based on this model we generated the Sub2 mutant Sub2-D302R (Supplementary Figs S7 and S8A), as the corresponding mutation in human DDX39B/UAP56 (D283R) abolishes the interaction with SARNP [36].

Sub2 and Sub2-D302R exhibited comparable unwinding and RNA-binding properties and a similar overall conformation as determined by HDX-MS (Fig. 2D and E, Supplementary Figs S8B and S9, and Supplementary Dataset 1). Furthermore, this mutation disrupts the interaction with the Tho1-CTD as intended, as shown by an electrophoretic mobility shift assay with 13 nt 6-FAM-labelled ssRNA and Sub2 (Supplementary Fig. S8C). Importantly, the helicase

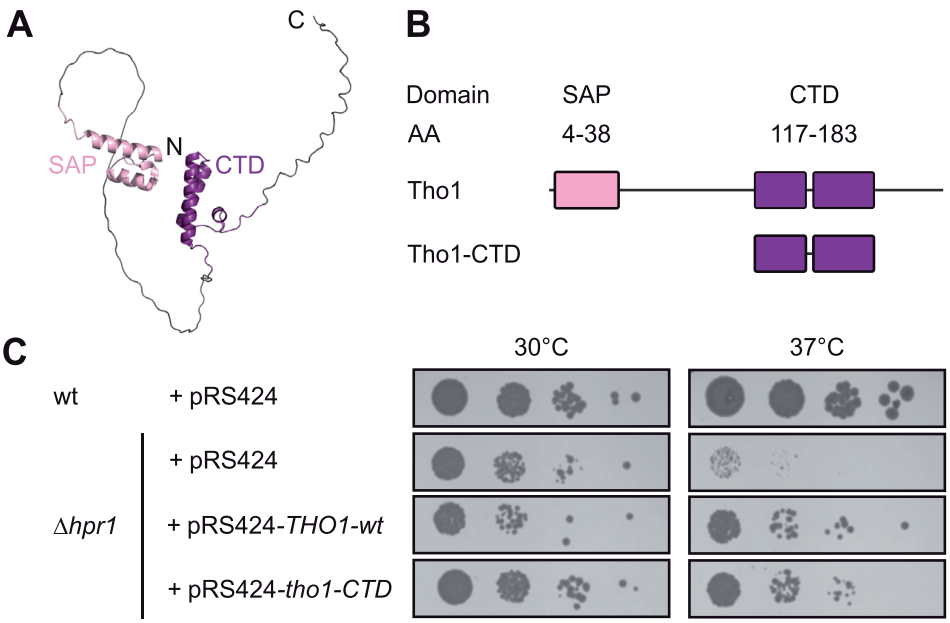

Figure 1. The CTD of Tho1 suppresses the growth defect of *Δhpr1* cells. (**A**) Structural model of full-length Tho1 predicted by AlphaFold (AF-P40040-F1). (**B**) Domain organization of Tho1. The Tho1-CTD truncation mutant consists of amino acids 117–183 and contains two conserved helical motifs (purple boxes). (**C**) Overexpression of the Tho1-CTD suppresses the growth defect of *Δhpr1* cells at 37°C as does full-length Tho1. Ten-fold serial dilutions of wild-type or *Δhpr1* cells overexpressing Tho1 or the Tho1-CTD from the high-copy plasmid pRS424 were spotted onto SDC (-trp) plates and grown for 3 days at the indicated temperatures. Wild-type and *Δhpr1* cells transformed with pRS424 served as positive and negative control, respectively. Representative result of three experiments.

activity of Sub2-D302R was no longer stimulated by the Tho1-CTD (Fig. 2E). Consequently, the direct interaction of Sub2 with the Tho1-CTD is essential for Sub2's stimulation.

An ssRNA tail is required for efficient stimulation of Sub2's unwinding activity by the Tho1-CTD

Sub2 and DDX39B/UAP56 also show helicase activity on RNA/DNA hybrids, a function that might be associated with R-loop resolution [8, 51]. This raises the question whether the Tho1-CTD also stimulates the unwinding of chimeric partial duplexes by Sub2 (Fig. 3 and Supplementary Fig. S10). As expected, a partial DNA/DNA duplex was not unwound by Sub2, and the Tho1-CTD had no influence on this (Supplementary Fig. S10B). Compared to the pdRNA substrate, Sub2 unwound RNA/RNA blunt-end and all hybrid substrates more efficiently, resulting in a rapid initial decrease in fluorescence signal that could not be captured using a plate reader. To nevertheless monitor the entire time course of the unwinding reaction, stopped-flow measurements were performed (Fig. 3A). For a DNA/RNA hybrid substrate containing an 3′ ssRNA tail, unwinding was further enhanced by the Tho1-CTD (Fig. 3B). A similar stimulation was observed for a DNA/RNA hybrid with an 5′ ssRNA tail (Supplementary Fig. S11). Interestingly, Sub2 unwound the corresponding RNA/DNA hybrid with an 3′ ssDNA tail even more rapidly than the DNA/RNA hybrid. However, in this case, the Tho1-CTD provided no significant stimulation (Fig. 3B).

To determine whether an ssRNA tail is required for stimulation, we tested the unwinding of duplexes without a tail (Fig. 3C and Supplementary Fig. S10). Sub2 unwound the RNA/RNA blunt-end duplex more efficiently than the pdRNA substrate, yet the stimulatory effect of the Tho1-CTD was significantly reduced. A similar pattern was observed for the DNA/RNA hybrid lacking an ssRNA tail. Interestingly, unwinding reactions of the RNA/DNA hybrid were nearly unaffected by the absence of a single-stranded tail. These findings indicate that while an ssRNA tail negatively impacts Sub2's intrinsic unwinding activity, this drawback can be overcome by the Tho1-CTD-mediated stimulation.

A structural model of the Sub2-Tho1-CTD complex bound to a partial duplex RNA

To get further insights into the molecular mechanism of how the Tho1-CTD and the 3′ ssRNA tail affect Sub2's RNA unwinding activity, AlphaFold 3 [52] was used to generate models of the 13/38 pdRNA with two Sub2 protomers and the Tho1-CTD (Fig. 4A and Supplementary Fig. 12). In these models, one Sub2 protomer was bound close to the 3′ end of the ssRNA tail of the longer RNA strand, whereas a second Sub2 protomer was associated with the same strand at the RNA/RNA duplex. The Tho1-CTD was positioned between the two Sub2 protomers, similar to the arrangement in the crystal structure reported by [36]. Sub2-D302R, which was not stimulated by the Tho1-CTD (Fig. 2), was fully impaired in its interaction with the Tho1-CTD. However, since the Tho1-CTD contains two interaction interfaces with Sub2, it remains unclear whether both are required for helicase stimulation. To investigate this, several Tho1-CTD mutants were generated, targeting highly conserved arginine residues critical for the interaction. In the first interaction motif, R139 was replaced by lysine (R139K) or aspartic acid (R139D), while in the second motif, R159 was mutated accordingly (R159K, R159D) (Fig. 4B and Supplementary Fig. S13A). All Tho1-CTD mutants failed to stimulate RNA unwinding by Sub2 (Fig. 4C and Supplementary Fig. S13B). Attempts to restore

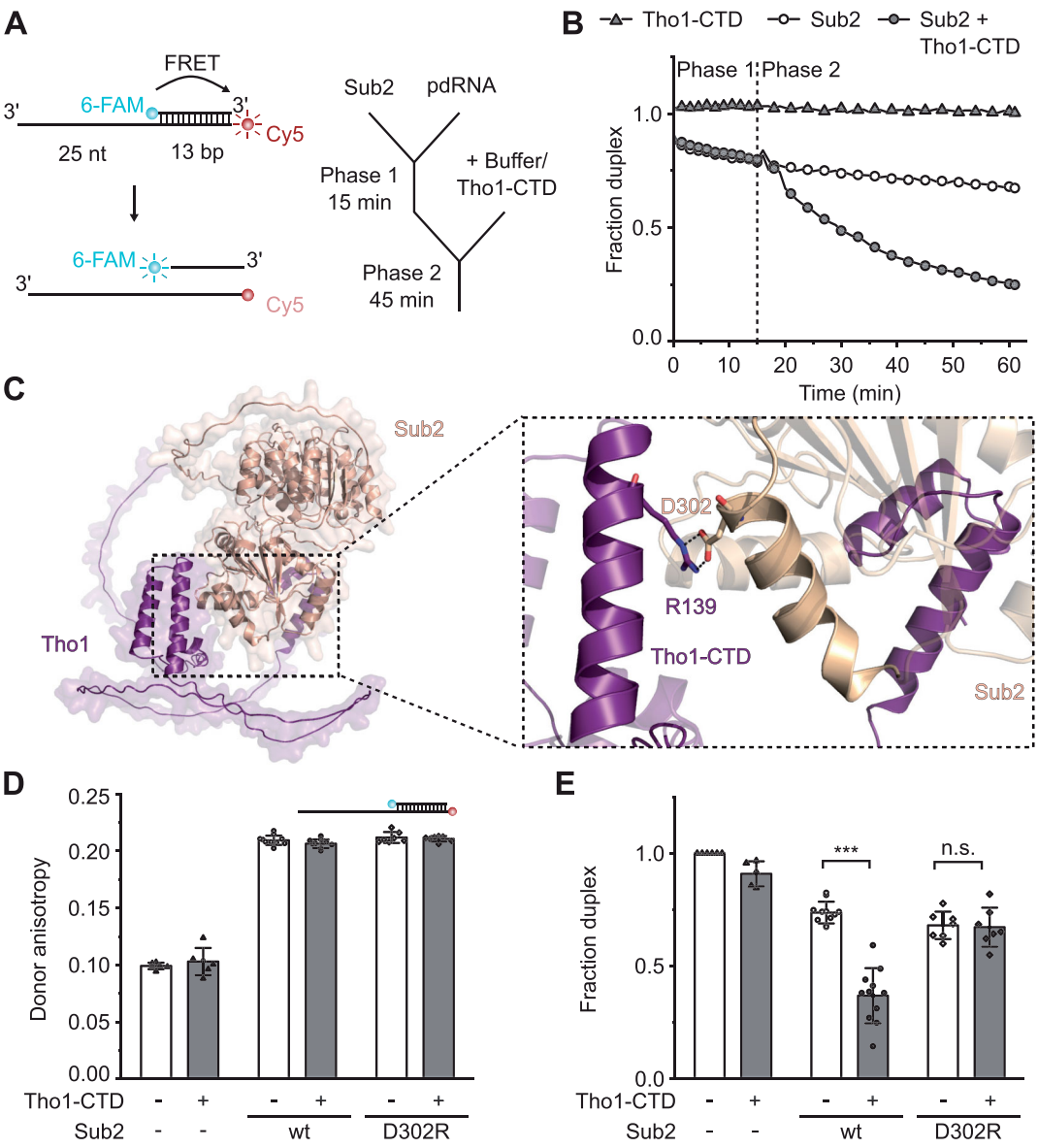

Figure 2. The Tho1-CTD stimulates Sub2's helicase activity by direct interaction. (**A**) Substrates and scheme of the FRET-based real-time unwinding assay. The donor dye 6-carboxyfluorescein (6-FAM) [49] and the acceptor dye Cy5 [48] are bound to the shorter top and the longer bottom strand of a pdRNA, respectively (Förster distance of 6.1 nm). (**B**) The Tho1-CTD stimulates Sub2's helicase activity. Unwinding of the pdRNA in the presence of Sub2 (1 μM) in the first phase of the measurement. Addition of 2 μM Tho1-CTD (filled symbols) in the second phase enhances Sub2-mediated unwinding. Representative result of $n = 11$ experiments. (**C**) Predicted Sub2-Tho1 interaction mediated by the Tho1-CTD (left) and a close-up of the interaction interface (right) (DOI: 10.5452/ma-bak-cepc-0534) [35]. Amino acids mutated in Sub2 (D302) and in the Tho1-CTD (R139) are depicted as sticks. (**D**) Sub2-D302R binds to pdRNA as efficiently as the wild-type protein. The Tho1-CTD cannot bind to RNA and does not change fluorescence anisotropy of RNA already bound by Sub2 or Sub2-D302R. pdRNA binding by 2 μM Tho1-CTD and 1 μM Sub2 or Sub2-D302R, in the absence or presence of 2 μM Tho1-CTD, is shown as fluorescence anisotropy of 6-FAM measured 20 min after the start of the reaction or 5 min after addition of the Tho1-CTD, respectively (see Supplementary Fig. S8 for experimental details). Mean ± SD from $n \geq 6$ experiments. (**E**) The helicase activity of Sub2-D302R is not stimulated by the Tho1-CTD. Unwinding of pdRNA by 1 μM Sub2 or Sub2-D302R in the absence or presence of the Tho1-CTD (2 μM). Mean ± SD of fraction duplex, calculated from FRET intensities after 60 min normalized to reactions without protein, from $n \geq 6$ experiments.

the stimulation by combining a Tho1-CTD-R139D/R159D mutant with the Sub2-D302R mutant were not successful (Supplementary Fig. S13B).

To test the *in vivo* function of our Tho1-CTD mutants, their ability to suppress the ts phenotype of *Δhpr1* cells was assessed. Due to highly variable protein levels when expressing the Tho1-CTD mutants from a plasmid, we integrated wild-type *THO1* and the different mutant alleles at the endogenous *THO1* locus in *Δhpr1* cells (Supplementary Figs S1 and S14A). This approach ensured stable protein expression of the Tho1-CTD and its mutants and allowed us to determine their functional effects in the absence of endogenous Tho1 (Supplementary Fig. S14 B and C). Overexpression of wild-type Tho1 and the Tho1-CTD from the endogenous locus successfully suppressed the ts phenotype. However, overexpression of either Tho1-CTD mutant (-R139K or -R159K) failed to restore growth at 37°C (Fig. 4D and Supplementary Fig. S14D and E). Taken together, our results demonstrate that single point mutations in Tho1-CTD's interface with Sub2 disrupt both Sub2 helicase stimulation *in vitro*

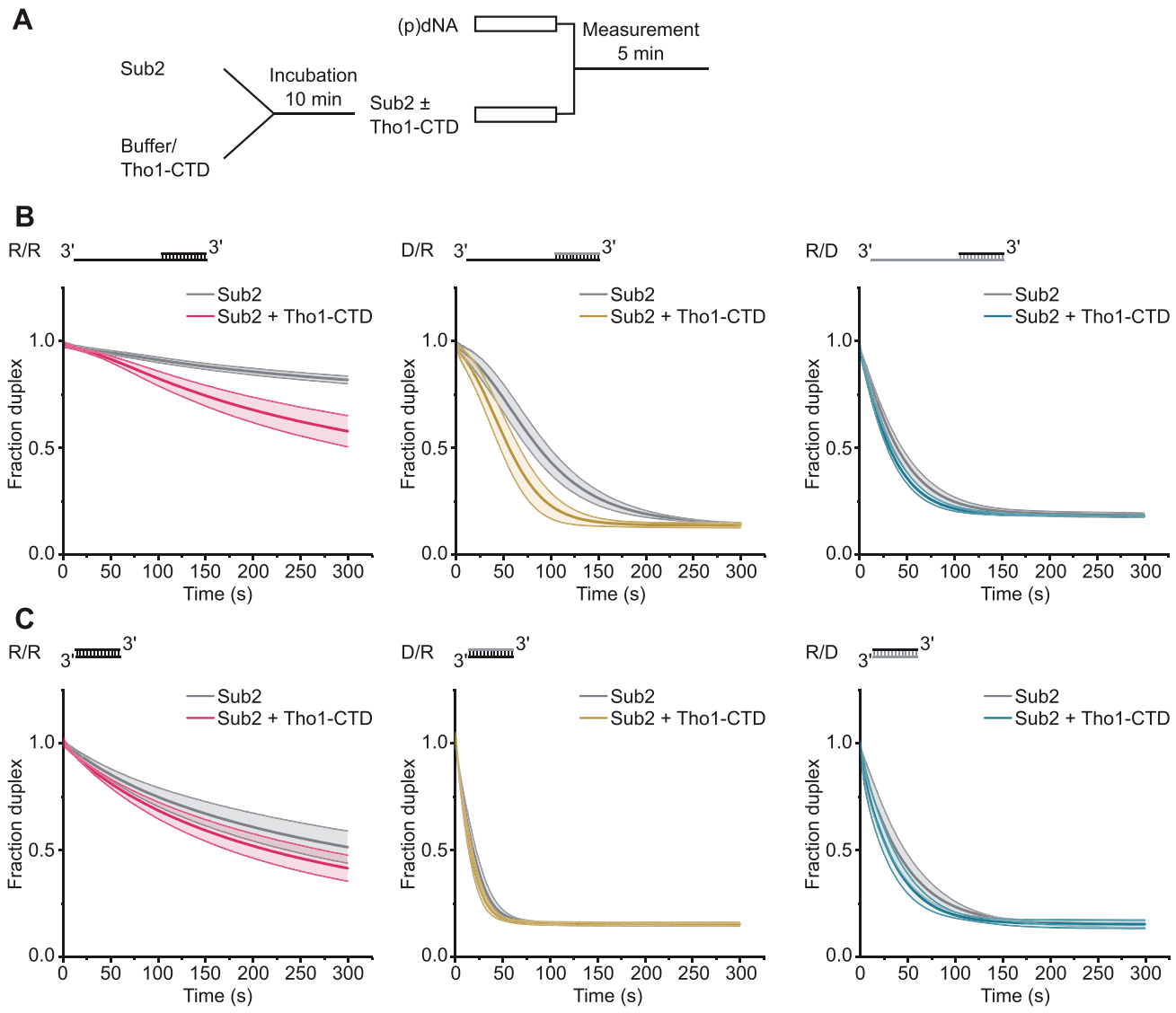

Figure 3. Stimulation of Sub2 unwinding activity by the Tho1-CTD depends on an ssRNA tail. (**A**) Scheme of the real-time unwinding assay performed using stopped-flow measurements. Substrates tested include RNA/RNA duplexes (R/R) or DNA/RNA hybrids (D/R and R/D). (**B**) Sub2-mediated unwinding is stimulated in the presence of an ssRNA but not by an ssDNA tail. Substrates consist of 13 bp duplexes with 25 nt 3′ single-stranded tails. (**C**) The Tho1-CTD only weakly stimulates unwinding of short 13 bp blunt-end duplexes. Unwinding by 1 μM Sub2 was measured in the absence or presence of 0.5 μM Tho1-CTD. Shown are the mean ± SD of $n = 3$ experiments.

and the Tho1-CTD's *in vivo* function, highlighting the importance of both conserved helical motifs within the Tho1-CTD.

Cross-species stimulation of UAP56 by the Tho1-CTD

The crystal structure of the yeast Tho1-CTD with human DDX39B/UAP56 implied a conserved interaction between these proteins [36]. Hence, we wondered whether *A. thaliana* UAP56, which was shown to be stimulated by the *Arabidopsis* Tho1 ortholog MOS11 [34], can also be stimulated by the Tho1-CTD. Based on an AlphaFold 3-generated structural model (Fig. 5A and Supplementary Fig. 15), an UAP56-D284R mutant was generated (corresponding to D302R in Sub2) (Supplementary Fig. S16). When compared in our helicase assay, the RNA helicase activity of wild-type UAP56 was stimulated by the Tho1-CTD, whereas unwinding of the UAP56-D284R mutant was not affected (Fig. 5B). Furthermore, stimulation of wild-type UAP56 was not observed with the Tho1-CTD mutants Tho1-CTD-R139D, Tho1-CTD-R159D, and Tho1-CTD-139D/R159D. In summary, these results indicate that the Tho1-CTD can stimulate UAP56 across species boundaries, in a manner that requires two intact helical motifs.

Helicase stimulation by the Tho1-CTD depends on a 2:1 complex

As Tho1-CTD mutants with a mutation in either of the two helical motifs do not stimulate Sub2/UAP56, we wondered whether they could still form a complex with one helicase while being deficient in binding to the second. The AlphaFold 3 model revealed a proximity between a non-conserved cysteine residue (Cys311) in UAP56 to several lysine residues of the Tho1-CTD at the protein-protein interface (Fig. 6A). We used chemical crosslinking as described in [47] with the

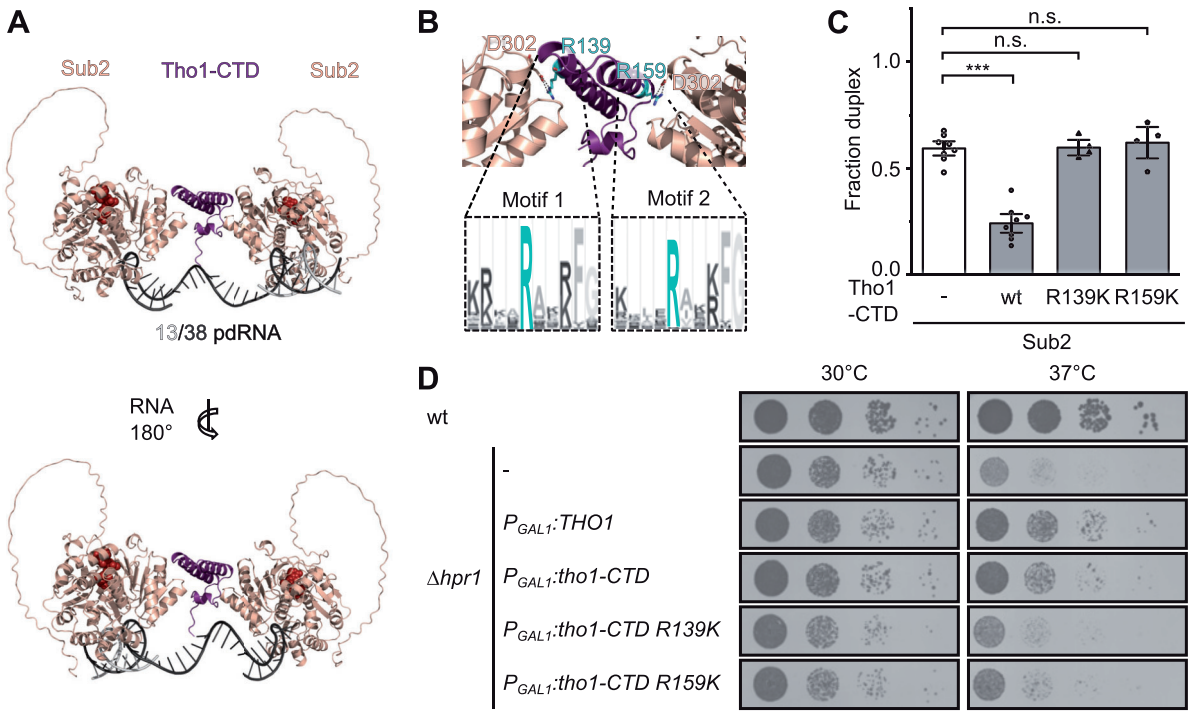

Figure 4. Both conserved helical motifs in the Tho1-CTD are required to stimulate Sub2 helicase activity. (**A**) AlphaFold 3 [52] prediction of a 2:1 complex consisting of Sub2 and the Tho1-CTD bound to the pdRNA substrate used for helicase assays. One Sub2 is bound to the duplex region and the second Sub2 to the single-stranded 3′ tail. ATP is shown in red. (**B**) Close-up of the interaction sites in panel (A). The Tho1-CTD contains two conserved sequence motifs, one in each helix (motif 1 and 2). The arginine residues within these motifs used for mutational analysis are highlighted in cyan. (**C**) Tho1-CTD mutants with an R-K mutation in motif 1 (R139K) or motif 2 (R159K) do not stimulate Sub2 unwinding. Shown is the fraction duplex after 60 min incubation with Sub2 (1 μM) in the absence or presence of the indicated Tho1-CTD mutants (2 μM), calculated from FRET intensities normalized to reactions without protein. Mean ± SD of $n \geq 3$ experiments. (**D**) Overexpression of the Tho1-CTD mutants fails to suppress the growth defect of *Δhpr1* cells at 37°C. Ten-fold serial dilutions of wild-type or *Δhpr1* cells overexpressing Tho1 or the Tho1-CTD from genomic integration of the indicated constructs at the *THO1* locus. Cells were grown for 3 days at the indicated temperatures. Wild-type and *Δhpr1* cells served as positive and negative control, respectively. Representative result of $n = 5$ experiments.

heterobifunctional crosslinker MTS-4-NHS that specifically targets thiol groups (cysteine residues) and primary amines (lysine residues) (Fig. 6B). Already in the absence of RNA, a new band appeared, indicating a crosslinked complex between UAP56 and Tho1-CTD (Fig. 6C). Addition of 38 nt RNA yielded additional bands suggesting the formation of higher-order complexes (Fig. 6C). Notably, these higher-order complexes did not form on shorter RNA (13 nt) (Supplementary Fig. S17). Liquid chromatography-mass spectrometry (LC–MS) analysis of the respective bands confirmed crosslinking of the Tho1-CTD to UAP56 (Supplementary Fig. S18 and Supplementary Dataset 2).

To dissect the specific contribution of each protein to the respective complexes, crosslinking experiments in the absence of individual components were performed. Omission of the Tho1-CTD resulted in the disappearance of the prominent smaller band and of some of the upper bands (Fig. 6D, compare lanes 2 and 6). The remaining upper bands in lane 6 likely represent intermolecular crosslinks forming between different UAP56 protomers, whereas the slight blurring of the lower band might be due to intramolecular UAP56 crosslinks. In the absence of UAP56, no additional bands were present (Fig. 6D, lanes 7–9). Thus, the two prominent bands marked by empty and filled triangles only appeared in the presence of both UAP56 and the Tho1-CTD. Their different migration behaviour suggested that the lower band (empty triangle) represented a 1:1 complex of UAP56 and Tho1-CTD, whereas the higher one (filled triangle) was a 2:1 complex with two UAP56 and one Tho1-CTD. However, it is difficult to estimate the stoichiometry from the apparent molecular mass since the mobility of crosslinked complexes is also influenced by the crosslink position in each of the proteins.

To circumvent this limitation, the impact of the Tho1-CTD interface mutations on crosslinking were tested. While the single point mutants (R139D or R159D) still yielded the lower complex, the upper complex was no longer discernible (Fig. 6E, lanes 3 and 4, respectively). For the double mutant (R139D/R159D), no UAP56-Tho1-CTD crosslink was observed (Fig. 6E, lane 5). Similarly, the D284R mutation in UAP56 prevented the formation of crosslinked complexes with the Tho1-CTD while still allowing the formation of intra-molecular crosslinks (Fig. 6E, lanes 7–9).

Finally, to rule out nonspecific crosslinking, we performed additional crosslink experiments with yeast Sub2. Sub2 contains six endogenous cysteine residues, but none of these are located near the Tho1-CTD interface. No crosslinked complexes were detectable for Sub2-wt with the Tho1-CTD beyond faint background bands (Supplementary Fig. S19). By contrast, introduction of a cysteine at the interface position corresponding to UAP56-C311 (Sub2-S329C) resulted in strong, well-defined crosslink bands that mirrored those observed for UAP56 (Supplementary Figs S7 and S19). This demonstrates that crosslinking occurs specifically at the Tho1-CTD interaction site, thereby substantiating the 2:1 complex

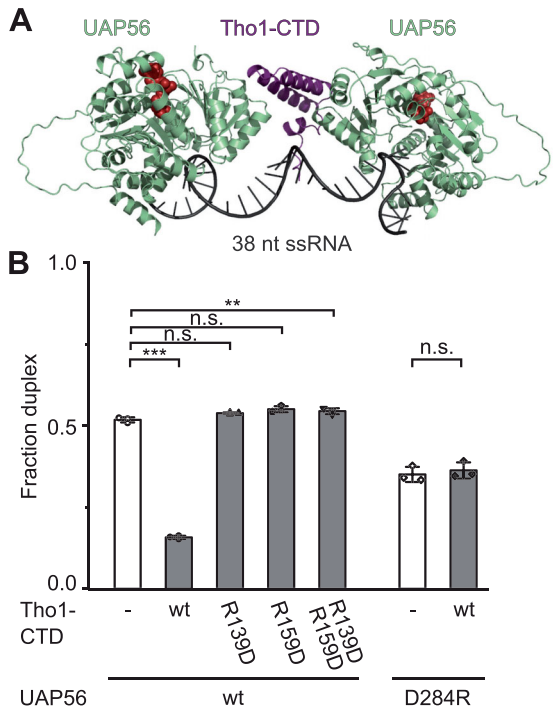

Figure 5. The *S. cerevisiae* Tho1-CTD stimulates *A. thaliana* helicase UAP56. (**A**) AlphaFold 3 [52] prediction of *A. thaliana* UAP56 and the *S. cerevisiae* Tho1-CTD 2:1 complex on a 38 nt RNA. ATP is shown in red. (**B**) Mutation of a single conserved helical motif in the Tho1-CTD abolishes UAP56 helicase stimulation. Effect of the Tho1-CTD wild-type and mutants with an R to D mutation in motif 1 (R139D), motif 2 (R159D) or both (R139D-R159D) on pdRNA unwinding of UAP56 and the interface mutant UAP56-D284R. Mean ± SD of fraction duplex, calculated from FRET intensities after 30 min normalized to reaction without protein from $n = 3$ experiments.

model and excluding unspecific oligomerization as the source of the observed bands.

Altogether, our data show that the Tho1-CTD single mutants can interact with one helicase protomer. Since they are nevertheless incapable of stimulating helicase activity (Fig. 4), these results confirm that a 1:1 interaction is not sufficient for stimulation, highlighting the importance of a 2:1 complex formation.

UAP56 stimulation by MOS11 also requires more than one motif

Having established that the Tho1-CTD stimulates both Sub2 and UAP56 helicase activity by promoting 2:1 complex formation, helicase assays were conducted using UAP56 and its cognate interaction partner MOS11. These experiments aimed to address whether the same principle applies to Tho1 orthologs with multiple and far-stretched conserved helical motifs, and whether this structural expansion influences specific aspects of the stimulation (Fig. 7A). Like the Tho1-CTD, MOS11 alone exhibited no helicase activity but strongly stimulated UAP56-mediated unwinding of a tailed RNA/RNA duplex (Fig. 7B). However, MOS11 showed an even stronger stimulation of UAP56 helicase activity on blunt-end RNA duplexes, a substrate that Tho1-CTD only weakly supported. The Tho1-CTD and MOS11 interact with the same UAP56 interface, as shown by the loss of stimulation in the UAP56-D284R mutant (Figs 5B and 6E and Supplementary Fig. S20). Therefore, the extended spectrum of substrates for which a stimulation can be observed must reflect intrinsic differences in the Tho1 ortholog beyond the interaction interface—most likely either the additional motifs in MOS11, the greater distance between these motifs, or a combination of both.

To examine the contribution of motif number to the observed stimulation on duplex RNA, we generated MOS11 mutants in which conserved arginine residues within individual motifs were replaced by lysines (Fig. 7C and Supplementary Fig. S21). All mutants retained RNA binding, indicating that the substitutions did not affect protein integrity (Supplementary Fig. S22). A variant with mutations in all five motifs (Mot. 0) failed to stimulate UAP56, demonstrating that the motifs are indeed essential for helicase stimulation. The mutant with only one intact motif (Mot. 1) showed no significant stimulation, analogous to the Tho1-CTD single-interface mutants that allowed only formation of a 1:1 complex and failed to support helicase activation. A mutant retaining only Mot. 1 + 2 slightly increased unwinding velocity, while inclusion of a third motif (Mot. 1–3) substantially enhanced unwinding velocity. The Mot. 1–4 mutant, containing four motifs, approached wild-type activity, suggesting that helicase stimulation progressively improves with the number of available MOS11 helical motifs.

Flexible spacing between motifs enhances stimulation

Because MOS11 differs from Tho1 not only in motif number but also in the length and flexibility of the interjacent linkers, the potential influence of motif spacing on helicase stimulation was examined. MOS11 variants with only two intact motifs at increasing distances (Mot. 1 + 2, Mot. 1 + 3, Mot. 1 + 4, Mot. 1 + 5) all retained RNA binding (Supplementary Figs S21 and S22). However, Mot. 1 + 2 provided only minimal helicase stimulation, and unwinding velocity progressively increased with greater spacing, peaking for Mot. 1 + 5 (Fig. 7D). This finding extended to a short RNA/DNA duplex, where MOS11 enabled UAP56 to unwind this hybrid duplex more efficiently (Supplementary Fig. S23). Efficient stimulation also required two intact motifs, with Mot. 1 + 5 being most efficient (Supplementary Fig. S23).

Together, these data demonstrate that MOS11, like the Tho1-CTD, relies on at least two intact helical motifs for helicase stimulation. However, unlike the Tho1-CTD, MOS11 offers the possibility to combine motifs located at various distances—a flexibility that appears to be advantageous for different substrates.

Discussion

From yeast to human, the TREX complex and its largest subcomplex, the THO complex, play crucial roles in mRNA splicing, 3′ end processing and nuclear mRNA export. Cells with a defective THO complex show a hyperrecombination phenotype and furthermore defects in nuclear mRNA export and growth, all of which are suppressed by overexpression of either the TREX component Sub2 or its interaction partner Tho1 [27, 31, 32]. Complex formation of Sub2 and Tho1 via the Tho1-CTD has been suggested based on modelling efforts [35]. In addition, a recent structural study presented a 2:1 complex formed by the human Sub2 ortholog DDX39B/UAP56 with the Tho1-CTD [36].

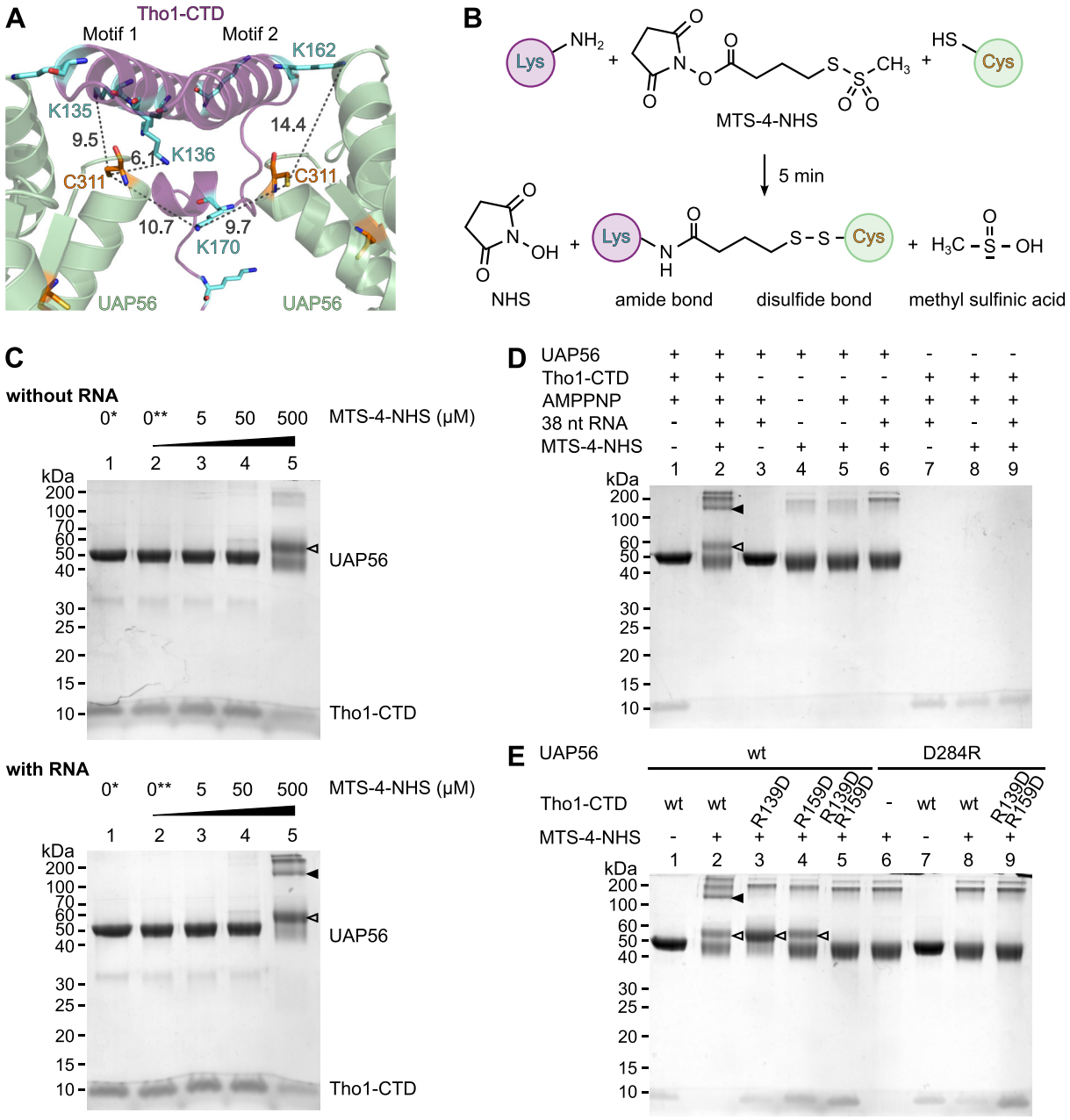

Figure 6. UAP56 and the Tho1-CTD form a 2:1 complex. (**A**) Zoom into the AlphaFold 3-predicted [52] structure of the UAP56-Tho1-CTD 2:1 complex with ssRNA (Fig. 5). Key residues involved in crosslinking are highlighted: cysteines in UAP56 (orange) and lysines in the Tho1-CTD (cyan). The distances between reactive groups are indicated in Å. (**B**) Scheme of the MTS-4-NHS crosslinking reaction. (**C**) UAP56 and the Tho1-CTD can be crosslinked using MTS-4-NHS. Coomassie gels of the crosslinking reactions between UAP56 and the Tho1-CTD with increasing concentrations of MTS-4-NHS in the absence (top) or presence (bottom) of 38 nt ssRNA. (**D**) UAP56 and the Tho1-CTD form two different intermolecular crosslinks. Coomassie gel of the crosslinking analysis in the absence of individual components. The presence or absence of UAP56, the Tho1-CTD, AMPPNP and RNA is indicated. (**E**) Tho1-CTD single mutants still interact with UAP56 but fail to form a 2:1 complex. Crosslinking analysis of UAP56 and the Tho1-CTD interface mutants. The presence of wild-type or mutant Tho1-CTD is indicated. All reactions were performed with 5 μM UAP56, 2.5 μM Tho1-CTD, 1 mM AMPPNP, 0.5 mM $MgCl_2$, and 2.5 μM RNA. Crosslinking was initiated by adding 500 μM MTS-4-NHS. Key: ∗ control with H_2O, ∗∗ control with solvent (DMSO), empty triangle: 1:1 UAP56-Tho1-CTD complex, filled triangle: 2:1 UAP56-Tho1-CTD complex. Representative results for $n = 3$ experiments.

In this study, we demonstrate that the Tho1-CTD alone is sufficient to suppress the ts phenotype of cells lacking the THO component Hpr1 (Fig. 1C) and to stimulate nucleic acid double-strand unwinding by the DEAD-box helicase Sub2 (Fig. 2E). This stimulation strictly depends on formation of the 2:1 complex between Sub2 and the Tho1-CTD, since a single point mutation in either one of the conserved Sub2 interaction motifs in the Tho1-CTD, restricting complex formation to a 1:1 stoichiometry (Figs 4B and 6), is sufficient to abolish stimulation (Fig. 4C). Importantly, the respective mutants also fail to suppress the growth defect of *Δhpr1* cells at 37°C (Fig. 4D), arguing for a physiological relevance not only of the Sub2-Tho1 interaction as such, but specifically of the 2:1 complex.

Our helicase assays with different substrates indicate that stimulation by the Tho1-CTD is most prominent on substrates

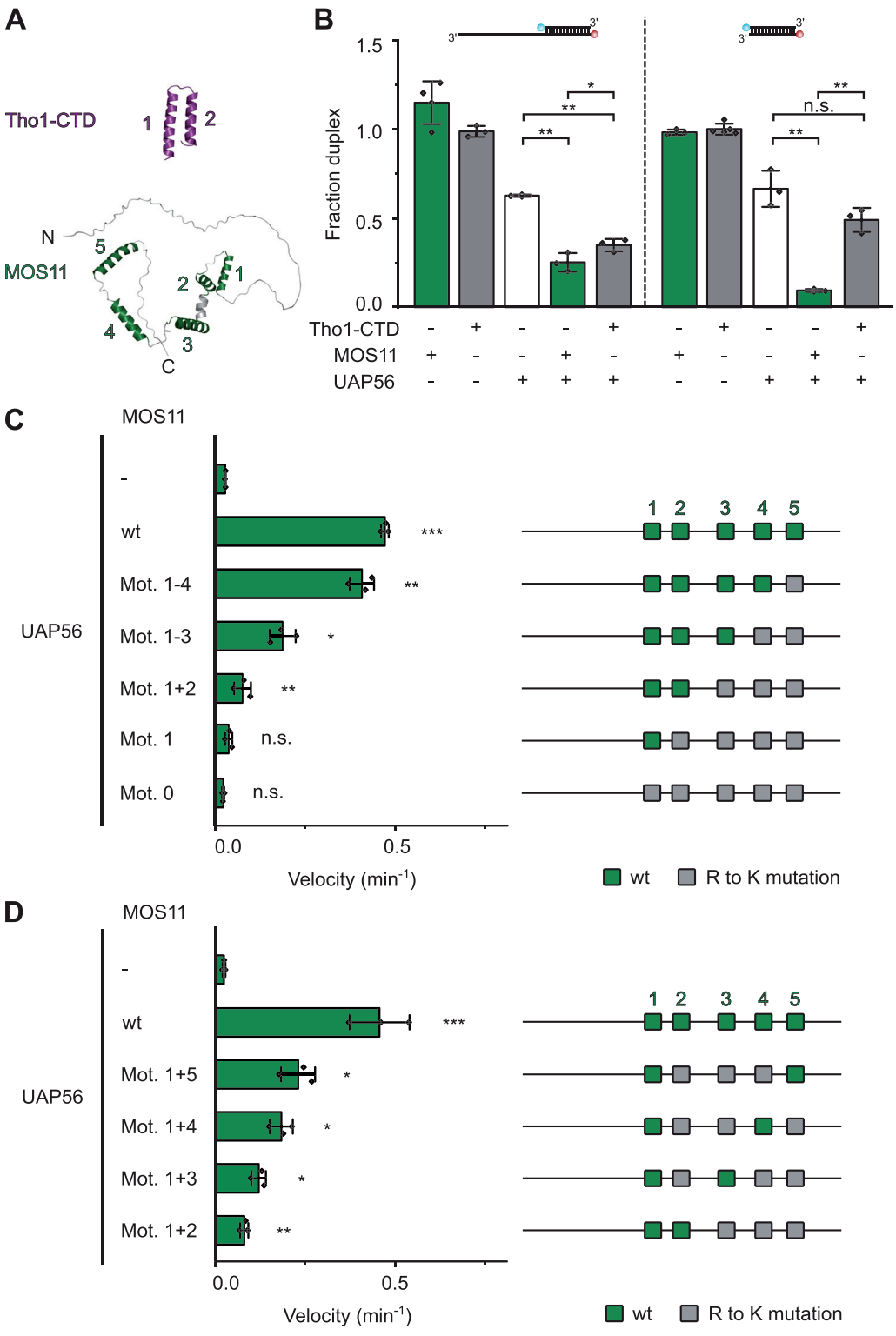

Figure 7. MOS11 stimulates UAP56 unwinding on a short duplex substrate. (**A**) Predicted structures of the Tho1-CTD (AF-P40040-F1) and MOS11 (AF-Q9LZ08-F1) highlighting their respective domains for helicase interaction. (**B**) MOS11 significantly stimulates unwinding by UAP56 in the absence of an ssRNA tail. Reactions were performed using either pdRNA substrates with a 25 nt single-stranded tail or 13 bp RNA duplexes. MOS11 alone does not exhibit unwinding activity. Shown is the fraction of substrate unwound after 10 min, as mean ± SD from $n = 3$ experiments. (**C**) More helical motifs lead to a stronger helicase stimulation. Unwinding velocity on a 13 bp RNA duplex of UAP56 alone or in the presence of wild-type MOS11 or MOS11 mutants in which different numbers of conserved arginine residues were replaced by lysines. (**D**) Increasing distance between the helical motifs enhances unwinding stimulation on 13 bp duplexes. Comparison of MOS11 mutants containing two intact motifs at different positions, with all other motifs being mutated. All reactions were performed with 1 μM of UAP56 and 2 μM of either wild-type Tho1-CTD, MOS11 or the respective MOS11 mutant. Shown are mean ± SD from $n = 3$ experiments.

with an ssRNA tail. On such substrates, unwinding by Sub2 alone is slow, but can be enhanced by addition of the Tho1-CTD (Fig. 3). Substrate preferences of Sub2 are not well defined, but other DEAD-box helicases are reported to favour binding to single-stranded RNA and often rely on single-stranded regions for loading onto the substrate and, consequently, for efficient unwinding [9, 10, 53, 54]. Our data suggest a similar ssRNA preference for Sub2; however, in our case, the presence of ssRNA appears to interfere with unwinding. Based on this observation, and the strict requirement of the 2:1 complex for stimulation, we propose that the Tho1-CTD stimulates Sub2's helicase activity by acting as a scaffold that promotes Sub2 oligomerization on RNA: In the absence of Tho1-CTD, Sub2's preference for ssRNA will frequently lead to competitive and non-productive binding to the single-stranded overhang of partial duplex substrates. If this ssRNA binding occurs close to the duplex, this may even cause steric hindrance impeding binding of a second protomer to the adjacent double-stranded region. Consequently, productive engagement with the duplex—and its unwinding—is less frequent, manifesting as slower overall unwinding in our helicase assay (Fig. 8A, left panel). In a 2:1 complex bridged by Tho1-CTD, on the other hand, one Sub2 protomer can bind to its preferred substrate ssRNA, while the second Sub2 protomer binds the less favoured dsRNA. Consequently, dsRNA strand separation is a much more frequent event, and unwinding in our helicase assays proceeds faster (Fig. 8 A, middle panel). However, when complex formation is restricted to a 1:1 stoichiometry due to mutation of either one of the Tho1-CTD interaction sites, the scaffolding effect and therewith the stimulation by the Tho1-CTD is abolished, and overall unwinding is slow again (Fig. 8 A, right panel).

This Tho1-CTD-mediated oligomerization of Sub2 is reminiscent of the self-oligomerization of other DEAD-box helicases that likewise enhances nucleic acid unwinding activity [11, 12, 55]. For example, *S. cerevisiae* Ded1 preferentially binds the single-stranded regions of pdRNA substrates [9], and while tails of 25 nt lengths can accommodate two Ded1 protomers and are optimal for unwinding of the adjacent duplex, substrates with shorter tails are unwound less efficiently [10, 56]. Mutational analysis demonstrated that Ded1 forms higher-order oligomers mediated by its 69 aa C-terminal tail. Ded1 mutants lacking this C-terminus still form dimers but not higher-order oligomers, and they show significantly lower unwinding activity on the pdRNA substrates than wild-type Ded1 [10]. Recent high-resolution optical tweezer experiments revealed that Ded1 unwinds 16 bp RNA hairpins with adjacent single-stranded RNA tails in a stepwise manner through successive assembly of multiple protomers, starting from the 3′ ssRNA tail [57]. The authors conclude that single-stranded regions increase the local concentration of Ded1, and subsequent oligomerization promotes binding of additional Ded1p protomers onto the adjacent duplex, ultimately leading to strand separation [9, 10, 57]. Stimulation of Sub2 helicase activity by the Tho1-CTD apparently is based on a very similar mechanisms, but instead of self-oligomerization, Sub2's oligomerization is bridged by the Tho1-CTD. However, whereas Ded1 forms higher-order oligomers [10], Sub2 oligomerization is limited to dimers since the Tho1-CTD comprises only two copies of the helical interaction motifs.

Interestingly, the Tho1 orthologs in *Schizosaccharomyces pombe* and *Drosophila melanogaster* possess three and four of these motifs, respectively, and *A. thaliana* MOS11 as well as human SARNP contain even five motifs [37, 58]. Furthermore, while the two motifs in Tho1 are connected by a short linker and arranged in a rather rigid helix-turn-helix-like fold, the motifs in the *S. pombe*, *D. melanogaster*, *Homo sapiens* [36], and *A. thaliana* (Fig. 7) orthologs are connected by more flexible linkers of various lengths. Both human SARNP and *A. thaliana* MOS11 stimulate the helicase activity of their respective Sub2 orthologs through a hitherto unknown mechanism [25, 26, 33, 34]. However, due to the high motif conservation, cross-species interactions could be observed between the yeast Tho1-CTD and the human Sub2 ortholog DDX39B/UAP56 [36], and between the yeast Tho1-CTD and the *A. thaliana* Sub2 ortholog UAP56 (Fig. 5). Furthermore, our AlphaFold 3-generated models of yeast Sub2 with its cognate partner Tho1-CTD and of *A. thaliana* UAP56 with the yeast Tho1-CTD (Figs 4–6) are almost identical to the homologous 2:1 complex of human DDX39B/UAP56 and the Tho1-CTD [36]. Also, stimulation of *A. thaliana* UAP56 helicase activity, just like Sub2 stimulation by the Tho1-CTD, requires more than one intact interaction motif in its cognate partner MOS11 (Fig. 7). Many observations thus point to a related mechanism underlying helicase stimulation in the homologous systems.

However, our helicase assays with *A. thaliana* UAP56 and MOS11 also suggest that (i) the more MOS11 helical motifs are available for interaction, the better the helicase stimulation (Fig. 7C); (ii) the degree of stimulation correlates with the spatial separation of these motifs (Fig. 7D); and (iii) MOS11 stimulates UAP56 helicase activity on a broader range of substrates, namely blunt-end RNA duplexes (Fig. 7B, right panel) and blunt-end RNA/DNA duplexes (Supplementary Fig. 23). Corresponding AlphaFold 3 predictions consistently showed a 2:1 complex in which two UAP56 protomers are connected by MOS11 via two of its interaction motifs. Interestingly, in nearly all models the UAP56 protomers were positioned on opposite strands of the duplex substrate (Supplementary Dataset 3). When we extended this analysis to the MOS11 mutants containing only two intact helical motifs, we found that larger distances between the motifs correlated with both an increased likelihood of the two UAP56 protomers binding to opposite strands and with an improvement in model quality. Based on these findings, we propose that the presence of multiple motifs, connected by longer and more flexible linkers, make MOS11 a more flexible scaffold and enables it to also bridge UAP56 protomers binding to opposite strands of a duplex substrate (Fig. 8B). In case of the RNA/DNA hybrid substrate, this arrangement implies that one of the two protomers interacts with the DNA strand—a surprising substrate for an RNA helicase. Nevertheless, even though UAP56 does not bind ssDNA, it does weakly interact with dsDNA [59]. Bridged by MOS11, one UAP56 protomer could thus bind to the RNA strand of the hybrid substrate, while the extended MOS11 scaffold brings the second protomer near the DNA strand, making DNA binding more likely. Moreover, the larger number of interaction motifs in MOS11 might even allow for higher-order oligomerization of UAP56 similar to Ded1 [10, 57].

Altogether, the scenario depicted in our model of the MOS11-UAP56 interaction (Fig. 8B) is reminiscent of the flexible configuration suggested for the human Tho1 ortholog SARNP and its interaction partner DDX39B/UAP56 on RNA [36], but also of the recently documented stimulatory effect of ALYREF on UAP56 in human and *A. thaliana* [34, 60]. Like Tho1, ALYREF contains two motifs for

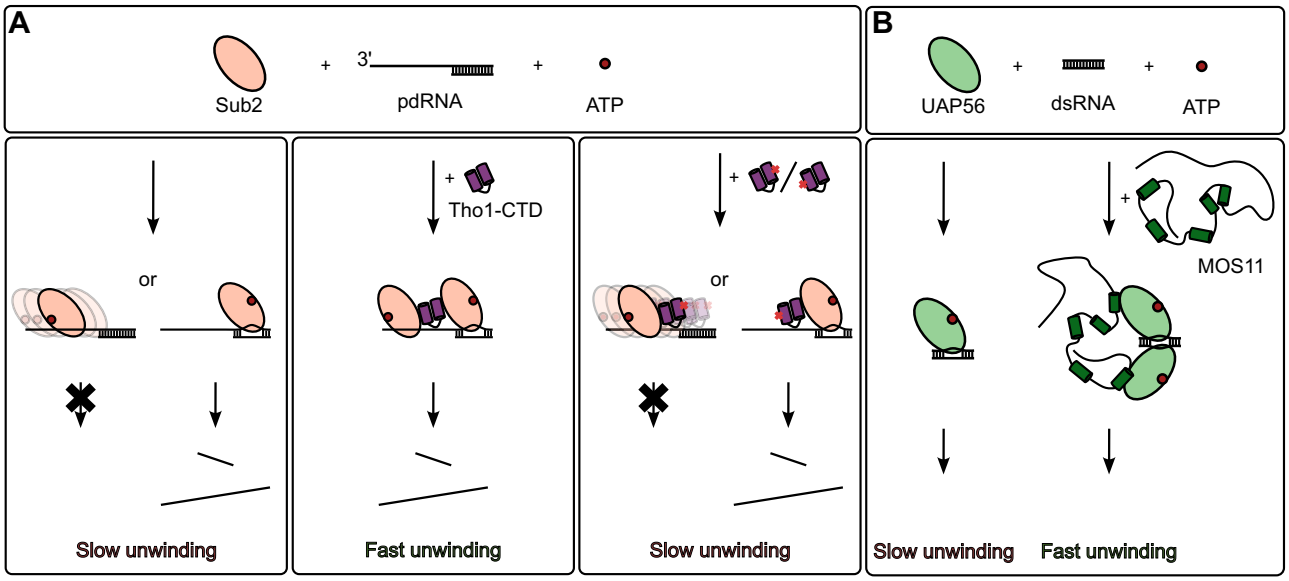

Figure 8. Model of Sub2/UAP56 helicase stimulation by the Tho1-CTD/MOS11 through helicase dimerization. **(A)** Sub2 monomers unwind pdRNA slowly since binding events to the single-stranded regions of the substrate are mostly unproductive (left panel). Interaction with the Tho1-CTD facilitates Sub2 dimerization on the RNA substrate and thereby enhances RNA unwinding (middle panel). Mutations in the Tho1-CTD preventing a 2:1 complex abolish this stimulation as dimerization of Sub2 is not facilitated (right panel). **(B)** MOS11 can stimulate RNA unwinding by promoting complex formation between RNA and two (or more) UAP56 protomers. The flexibility of the linkers and the number of motifs determine the efficiency of unwinding stimulation.

interaction with UAP56 [20, 38, 61]. However, its structural organization rather resembles the flexible arrangement observed in MOS11 or SARNP [36]. These similarities raise the possibility of a shared mechanism underlying helicase stimulation. In addition, ALYREF has been shown to cooperate with DDX39B/UAP56 in R-loop resolution, a process that depends on ALYREF's ability to bind nucleic acids [60]. Notably, full-length Tho1, MOS11 and SARNP also possess nucleic acid-binding activity [27, 34, 36]. Furthermore, deletion of MOS11 and depletion of SARNP have been shown to affect mainly the export of mRNAs with a high GC content—regions that are particularly prone to R-loop formation [34, 36]. Given that Tho1/SARNP and ALYREF can engage with DDX39B/UAP56 simultaneously via distinct interaction sites on the helicase [36], it is conceivable that the contribution of the Tho1 protein family to R-loop resolution or nuclear mRNA export is based on their interaction either with DDX39B/UAP56 alone or in cooperation with ALYREF.

In summary, we uncover an evolutionary conserved mechanism by which Tho1-family proteins stimulate the nucleic acid unwinding activity of yeast Sub2 and *A. thaliana* UAP56 DEAD-box helicases through a scaffolding function that mediates helicase oligomerization. The number of motifs and the flexibility of the connecting linkers appear to define the scaffold's reach, thereby influencing both the range of substrates that can be unwound and the potential degree of helicase oligomerization. Together with the *in vivo* requirement of two intact motifs in the Tho1-CTD for suppression of the THO-complex mutant growth defect, our *in vitro* and *in silico* results thus establish a cofactor-mediated mode of helicase stimulation that is both physiologically relevant and mechanistically versatile.

Acknowledgements

We are thankful to Maren Brücks, Amelie Müller, and Jan Kohlert for their assistance with the experiments. We thank Karl-Heinz Kogel for kindly providing the cDNA encoding UAP56 and MOS11 used in this study. We thank Tina Krieg and Uwe Linne (Philipps University Marburg) for the identification of proteins from crosslinks by mass spectrometry. We acknowledge the support by the Deutsche Forschungsgemeinschaft (DFG, German Research Foundation) to the core facility for HDX-MS (project numbers 260989694 and 324652314) to Gert Bange, Philipps University Marburg. AI assistance (ChatGPT-4) was used for language improvements.

Author contributions: Fabienne Becker (Conceptualization [equal], Investigation [lead], Methodology [equal], Validation [equal], Visualization [lead], Writing – original draft [equal], Writing – review & editing [equal]), Matthias Bastian Miosga (Conceptualization [supporting], Investigation [supporting]), Minhaz Mannan (Investigation [supporting]), Vera Bettenworth (Project administration [supporting], Writing – original draft [supporting], Writing – review & editing [supporting]), Wieland Steinchen (Formal analysis [supporting], Investigation [supporting], Methodology [supporting], Visualization [supporting], Writing – original draft [supporting], Writing – review & editing [supporting]), Katja Sträßer (Conceptualization [supporting], Funding acquisition [equal], Resources [equal], Supervision [supporting], Writing – review & editing [equal]), and Peter Friedhoff (Conceptualization [lead], Formal analysis [equal], Funding acquisition [equal], Investigation [supporting], Methodology [supporting], Project administration [lead], Resources [equal], Supervision [lead], Writing – original draft [equal])

Supplementary data

Supplementary data is available at NAR online.

Conflict of interest

None declared.

Funding

This work was supported by the DFG (Deutsche Forschungsgemeinschaft) grant GRK2355 to P.F. and K.S. Funding to pay the Open Access publication charges for this article was provided by DFG project 325443116.

Data availability

The data underlying this article are available in the article and in its online supplementary material.

References

1. Linder P, Jankowsky E. From unwinding to clamping—the DEAD box RNA helicase family. *Nat Rev Mol Cell Biol* 2011;12:505–16. https://doi.org/10.1038/nrm3154
2. Taschuk F, Cherry S. DEAD-Box helicases: sensors, regulators, and effectors for antiviral defense. *Viruses* 2020;12:181. https://doi.org/10.3390/v12020181 .
3. Venus S, Jankowsky E. Measuring the impact of cofactors on RNA helicase activities. *Methods* 2022;204:376–85. https://doi.org/10.1016/j.ymeth.2022.04.005
4. Hilbert M, Karow AR, Klostermeier D. The mechanism of ATP-dependent RNA unwinding by DEAD box proteins. *Biol Chem* 2009;390:1237–50. https://doi.org/10.1515/BC.2009.135
5. Rogers GW, Jr., Lima WF, Merrick WC. Further characterization of the helicase activity of eIF4A. Substrate specificity. *J Biol Chem* 2001;276:12598–608. https://doi.org/10.1074/jbc.M007560200
6. Shen J, Zhang L, Zhao R. Biochemical characterization of the ATPase and helicase activity of UAP56, an essential pre-mRNA splicing and mRNA export factor. *J Biol Chem* 2007;282:22544–50. https://doi.org/10.1074/jbc.M702304200
7. Jarmoskaite I, Russell R. DEAD-box proteins as RNA helicases and chaperones. *WIREs RNA* 2011;2:135–52. https://doi.org/10.1002/wrna.50
8. Perez-Calero C, Bayona-Feliu A, Xue X *et al.* UAP56/DDX39B is a major cotranscriptional RNA-DNA helicase that unwinds harmful R loops genome-wide. *Genes Dev* 2020;34:898–912. https://doi.org/10.1101/gad.336024.119
9. Yang Q, Jankowsky E. The DEAD-box protein Ded1 unwinds RNA duplexes by a mode distinct from translocating helicases. *Nat Struct Mol Biol* 2006;13:981–6. https://doi.org/10.1038/nsmb1165
10. Putnam AA, Gao Z, Liu F *et al.* Division of labor in an oligomer of the DEAD-box RNA helicase Ded1p. *Mol Cell* 2015;59:541–52. https://doi.org/10.1016/j.molcel.2015.06.030
11. Kinoshita Y, Murakami R, Muto N *et al.* Heterogeneous dissociation process of truncated RNAs by oligomerized Vasa helicase. *Commun Biol* 2021;4:1386. https://doi.org/10.1038/s42003-021-02918-0
12. Marcaida MJ, Kauzlaric A, Duperrex A *et al.* The human RNA helicase DDX21 presents a dimerization interface necessary for helicase activity. *iScience* 2020;23:101811. https://doi.org/10.1016/j.isci.2020.101811
13. Marintchev A, Edmonds KA, Marintcheva B *et al.* Topology and regulation of the human eIF4A/4G/4H helicase complex in translation initiation. *Cell* 2009;136:447–60. https://doi.org/10.1016/j.cell.2009.01.014
14. Dossani ZY, Weirich CS, Erzberger JP *et al.* Structure of the C-terminus of the mRNA export factor Dbp5 reveals the interaction surface for the ATPase activator Gle1. *Proc Natl Acad Sci USA* 2009;106:16251–6. https://doi.org/10.1073/pnas.0902251106
15. Montpetit B, Thomsen ND, Helmke KJ *et al.* A conserved mechanism of DEAD-box ATPase activation by nucleoporins and InsP6 in mRNA export. *Nature* 2011;472:238–42. https://doi.org/10.1038/nature09862
16. Libri D, Graziani N, Saguez C *et al.* Multiple roles for the yeast SUB2/yUAP56 gene in splicing. *Genes Dev* 2001;15:36–41. https://doi.org/10.1101/gad.852101
17. Rougemaille M, Dieppois G, Kisseleva-Romanova E *et al.* THO/Sub2p functions to coordinate 3′-end processing with gene-nuclear pore association. *Cell* 2008;135:308–21. https://doi.org/10.1016/j.cell.2008.08.005
18. Katahira J. mRNA export and the TREX complex. *Biochim Biophys Acta Gene Regul Mech* 2012;1819:507–13. https://doi.org/10.1016/j.bbagrm.2011.12.001
19. Strasser K, Hurt E. Splicing factor Sub2p is required for nuclear mRNA export through its interaction with Yra1p. *Nature* 2001;413:648–52. https://doi.org/10.1038/35098113
20. Strasser K, Masuda S, Mason P *et al.* TREX is a conserved complex coupling transcription with messenger RNA export. *Nature* 2002;417:304–8. https://doi.org/10.1038/nature746
21. Hurt E, Luo MJ, Rother S *et al.* Cotranscriptional recruitment of the serine-arginine-rich (SR)-like proteins Gbp2 and Hrb1 to nascent mRNA via the TREX complex. *Proc Natl Acad Sci USA* 2004;101:1858–62. https://doi.org/10.1073/pnas.0308663100
22. Chavez S, Beilharz T, Rondon AG *et al.* A protein complex containing Tho2, Hpr1, Mft1 and a novel protein, Thp2, connects transcription elongation with mitotic recombination in Saccharomyces cerevisiae. *EMBO J* 2000;19:5824–34. https://doi.org/10.1093/emboj/19.21.5824
23. Jimeno S, Rondon AG, Luna R *et al.* The yeast THO complex and mRNA export factors link RNA metabolism with transcription and genome instability. *EMBO J* 2002;21:3526–35. https://doi.org/10.1093/emboj/cdf335
24. Ren Y, Schmiege P, Blobel G. Structural and biochemical analyses of the DEAD-box ATPase Sub2 in association with THO or Yra1. *eLife* 2017;6 e20070.https://doi.org/10.7554/eLife.20070
25. Chang CT, Hautbergue GM, Walsh MJ *et al.* Chtop is a component of the dynamic TREX mRNA export complex. *EMBO J* 2013;32:473–86. https://doi.org/10.1038/emboj.2012.342
26. Sugiura T, Sakurai K, Nagano Y. Intracellular characterization of DDX39, a novel growth-associated RNA helicase. *Exp Cell Res* 2007;313:782–90. https://doi.org/10.1016/j.yexcr.2006.11.014
27. Jimeno S, Luna R, Garcia-Rubio M *et al.* Tho1, a novel hnRNP, and Sub2 provide alternative pathways for mRNP biogenesis in yeast THO mutants. *Mol Cell Biol* 2006;26:4387–98. https://doi.org/10.1128/MCB.00234-06
28. Germain H, Qu N, Cheng YT *et al.* MOS11: a new component in the mRNA export pathway. *PLoS Genet* 2010;6: e1001250.https:// doi.org/ 10.1371/ journal.pgen.1001250
29. Fukuda S, Wu DW, Stark K *et al.* Cloning and characterization of a proliferation-associated cytokine-inducible protein, CIP29. *Biochem Biophys Res Commun* 2002;292:593–600. https:// doi.org/ 10.1006/ bbrc.2002.6680
30. Choong ML, Tan LK, Lo SL *et al.* An integrated approach in the discovery and characterization of a novel nuclear protein over-expressed in liver and pancreatic tumors. *FEBS Lett* 2001;496:109–16. https://doi.org/10.1016/S0014-5793(01)02409-7
31. Piruat JI, Aguilera A. A novel yeast gene, THO2, is involved in RNA pol II transcription and provides new evidence for transcriptional elongation-associated recombination. *EMBO J* 1998;17:4859–72. https://doi.org/10.1093/emboj/17.16.4859
32. Fan HY, Merker RJ, Klein HL. High-copy-number expression of Sub2p, a member of the RNA helicase superfamily, suppresses

hpr1-mediated genomic instability. *Mol Cell Biol* 2001;21:5459–70. https://doi.org/10.1128/MCB.21.16.5459-5470.2001
33. Dufu K, Livingstone MJ, Seebacher J *et al.* ATP is required for interactions between UAP56 and two conserved mRNA export proteins, Aly and CIP29, to assemble the TREX complex. *Genes Dev* 2010;24:2043–53. https://doi.org/10.1101/gad.1898610
34. Rodel A, Weig I, Tiedemann S *et al.* Arabidopsis mRNA export factor MOS11: molecular interactions and role in abiotic stress responses. *New Phytol* 2024;243:180–94. https://doi.org/10.1111/nph.19773
35. Humphreys IR, Pei J, Baek M *et al.* Computed structures of core eukaryotic protein complexes. *Science* 2021;374:eabm4805. https://doi.org/10.1126/science.abm4805
36. Xie Y, Gao S, Zhang K *et al.* Structural basis for high-order complex of SARNP and DDX39B to facilitate mRNP assembly. *Cell Rep* 2023;42:112988. https://doi.org/10.1016/j.celrep.2023.112988
37. Jacobsen JO, Allen MD, Freund SM *et al.* High-resolution NMR structures of the domains of *Saccharomyces cerevisiae* Tho1. *Acta Crystallogr F Struct Biol Commun* 2016;72:500–6. https://doi.org/10.1107/S2053230X16007597
38. Hohmann U, Graf M, Tirián L *et al.*, An ATP-gated molecular switch orchestrates human mRNA export *Nature* 2025. https://doi-org.ezproxy.uni-giessen.de/10.1038/s41586-025-09832-z
39. Petropavlovskiy AA, Tauro MG, Lajoie P *et al.* A quantitative imaging-based protocol for yeast growth and survival on agar plates. *STAR Protocols* 2020;1:100182. https://doi.org/10.1016/j.xpro.2020.100182
40. Zadali R, Tomecki R, Topf U. Ribosomal protein Rps29/uS14 contributes to 18S rRNA maturation and its abundance regulates osmotic stress response in *S. cerevisiae*. *Nucleic Acids Res* 2025;53:gkaf807.https://doi.org/10.1093/nar/gkaf807
41. Karakasili E, Burkert-Kautzsch C, Kieser A *et al.* Degradation of DNA damage-independently stalled RNA polymerase II is independent of the E3 ligase Elc1. *Nucleic Acids Res* 2014;42:10503–15. https://doi.org/10.1093/nar/gku731
42. Putnam AA, Jankowsky E. AMP sensing by DEAD-box RNA helicases. *J Mol Biol* 2013;425:3839–45. https://doi.org/10.1016/j.jmb.2013.05.006
43. Ma WK, Cloutier SC, Tran EJ. The DEAD-box protein Dbp2 functions with the RNA-binding protein Yra1 to promote mRNP assembly. *J Mol Biol* 2013;425:3824–38. https://doi.org/10.1016/j.jmb.2013.05.016
44. Ordabayev YA, Nguyen B, Niedziela-Majka A *et al.* Regulation of UvrD helicase activity by MutL. *J Mol Biol* 2018;430:4260–74. https://doi.org/10.1016/j.jmb.2018.08.022
45. Hellenkamp B, Schmid S, Doroshenko O *et al.* Precision and accuracy of single-molecule FRET measurements—a multi-laboratory benchmark study. *Nat Methods* 2018;15:669–76. https://doi.org/10.1038/s41592-018-0085-0
46. Andreou AZ, Harms U, Klostermeier D. Single-stranded regions modulate conformational dynamics and ATPase activity of eIF4A to optimize 5′-UTR unwinding. *Nucleic Acids Res* 2019;47:5260–75. https://doi.org/10.1093/nar/gkz254
47. Storozhuk O, Bruekner SR, Paul A *et al.* MutL activates UvrD by interaction between the MutL C-terminal domain and the UvrD 2B domain. *J Mol Biol* 2024;436:168589. https://doi.org/10.1016/j.jmb.2024.168589
48. Olejko L, Bald I. FRET efficiency and antenna effect in multi-color DNA origami-based light harvesting systems. *RSC Adv* 2017;7:23924–34. https://doi.org/10.1039/C7RA02114C
49. Samatanga B, Andreou AZ, Klostermeier D. Allosteric regulation of helicase core activities of the DEAD-box helicase YxiN by RNA binding to its RNA recognition motif. *Nucleic Acids Res* 2017;45:1994–2006.
50. Michel BY, Dziuba D, Benhida R *et al.* Probing of nucleic acid structures, dynamics, and interactions with environment-sensitive fluorescent labels. *Front Chem* 2020;8:23. https://doi.org/10.3389/fchem.2020.00112
51. Saguez C, Gonzales FA, Schmid M *et al.* Mutational analysis of the yeast RNA helicase Sub2p reveals conserved domains required for growth, mRNA export, and genomic stability. *RNA* 2013;19:1363–71. https://doi.org/10.1261/rna.040048.113
52. Abramson J, Adler J, Dunger J *et al.* Accurate structure prediction of biomolecular interactions with AlphaFold 3. *Nature* 2024;630:493–500. https://doi.org/10.1038/s41586-024-07487-w
53. Song H, Ji X. The mechanism of RNA duplex recognition and unwinding by DEAD-box helicase DDX3X. *Nat Commun* 2019;10:3085. https://doi.org/10.1038/s41467-019-11083-2
54. Toyama Y, Shimada I. NMR characterization of RNA binding property of the DEAD-box RNA helicase DDX3X and its implications for helicase activity. *Nat Commun* 2024;15:3303. https://doi.org/10.1038/s41467-024-47659-w
55. Klostermeier D, Rudolph MG. A novel dimerization motif in the C-terminal domain of the *Thermus thermophilus* DEAD box helicase Hera confers substantial flexibility. *Nucleic Acids Res* 2009;37:421–30. https://doi.org/10.1093/nar/gkn947
56. Yang Q, Del Campo M, Lambowitz AM *et al.* DEAD-box proteins unwind duplexes by local strand separation. *Mol Cell* 2007;28:253–63. https://doi.org/10.1016/j.molcel.2007.08.016
57. Patrick EM, Yadav R, Senanayake K *et al.* High-resolution fleezers reveal duplex opening and stepwise assembly by an oligomer of the DEAD-box helicase Ded1p. *Nat Commun* 2025;16:1015. https://doi.org/10.1038/s41467-024-54955-y
58. Liao QQ, Shu X, Sun W *et al.* Capturing protein-protein interactions with acidic amino acids reactive cross-linkers. *Small* 2024;20:e2308383. https://doi.org/10.1002/smll.202308383
59. Kammel C, Thomaier M, Sorensen BB *et al.* Arabidopsis DEAD-box RNA helicase UAP56 interacts with both RNA and DNA as well as with mRNA export factors. *PLoS One* 2013;8:e60644. https://doi.org/10.1371/journal.pone.0060644
60. Bhandari J, Guillen-Mendoza C, Banks K *et al.* The molecular chaperone ALYREF promotes R-loop resolution and maintains genome stability. *J Biol Chem* 2024;300:107996. https://doi.org/10.1016/j.jbc.2024.107996
61. Heath CG, Viphakone N, Wilson SA. The role of TREX in gene expression and disease. *Biochem J* 2016;473:2911–35. https://doi.org/10.1042/BCJ20160010

Received: March 18, 2025. **Revised:** December 8, 2025. **Accepted:** December 18, 2025